Effect of low temperature tensile properties on crack driving force for Arctic applications

B.A. Dahl[a], X.B. Ren[a,b], O.M. Akselsen[a,b], B. Nyhus[b], Z.L. Zhang[c,*]

[a] *Department of Engineering Design and Materials, NTNU, N-7491, Trondheim, Norway*
[b] *SINTEF Materials and Chemistry, N-7465, Trondheim, Norway*
[c] *Department of Structural Engineering, NTNU, N-7491, Trondheim, Norway*

Abstract

Many petroleum companies expand their activities further north towards the Arctic region, resulting in design temperatures down to $-60\,^{\circ}\mathrm{C}$, which is much lower than what is usual for most current petroleum installations. As properties of steels are temperature dependent, it is of great interest to evaluate the effects of low temperature on the crack driving force in steels. The present work investigates these effects numerically using a finite element model of a single-edge-notched-tension (SENT) specimen with crack depth $a/W = 0.5$. The effects of Lüders strain and yield strength are studied for gross stress levels $\sigma_G/\sigma_y \leq 0.5$, and it is shown that an increase in yield strength and Lüders strain, as a result of Arctic temperature, intensifies the crack driving force. An approximate model that can be used to estimate the crack driving force based on yield strength, Lüders strain and loading is proposed.

Keywords: Arctic materials, crack driving force, Lüders plateau, low temperature, tensile properties

1. Introduction

The exploitation of hydrocarbons is continuously moving into new areas and harsher environments. Many petroleum companies are expanding their

*Corresponding author
Email address: zhiliang.zhang@ntnu.no (Z.L. Zhang)

activities further north, where a considerable part of the undiscovered oil and gas resources is expected to exist [1]. Consequently the structures built must be able to withstand the low temperatures present in the Arctic climate. Most structural materials have different behavior in such low temperatures, and this must be accounted for when designing and constructing structures to avoid accidents related to structural failure.

Much research has been carried out to study the behavior of steels in changing temperatures. The most obvious temperature dependent parameter is the yield strength, which for most steels increase with decreasing temperature [2–14]. Another temperature dependent property is the ductile-to-brittle transition (DBT) in steels. Due to the DBT, many steels become brittle when the temperature is sufficiently decreased, but the DBT is however not in the scope of this study.

Many steels, and also other materials, experience so-called Lüders and Lüders-like instabilities. These instabilities are associated with unpinning of dislocations from nitrogen and carbon atmospheres and dislocation multiplication, and they result in macroscopic inhomogeneous deformation [8, 15–20]. The Lüders instability is in uniaxial tensile tests observed as nearly horizontal stress plateaus, called Lüders plateaus, in the stress-strain curves after reaching the elastic limit of the material. This instability can be physically observed as localized deformation bands, called Lüders bands, propagating on the surface of uniaxial tensile tests. Structural steels often show this behavior. The amount of plastic straining occurring due to the Lüders instability is often called Lüders strain. Studies have shown that the Lüders strain is both rate and temperature dependent, and decreasing temperature is often associated with larger Lüders strain [7–9, 18, 21].

The fracture toughness of a material is often measured by using fracture mechanics tests, and is described by a single parameter, such as a critical stress intensity factor (K), crack tip opening displacement (CTOD, δ) or J-integral, depending on if it is a linear elastic or elastoplastic dominated fracture. The fracture toughness of steels is usually reduced when decreasing the temperature

[5, 10, 12–14, 22].

The fracture toughness can be interpreted as a measure of the ability of a material to resist fracture, while the crack driving force, on the other hand, can be defined as the force which opens the crack. The fracture toughness can be regarded as the critical level of crack driving force, and the same way as a critical CTOD can be a measure of the fracture toughness, the CTOD is often used as a measure of the crack driving force which changes with loading. Due to temperature dependent material parameters, decreasing temperature is assumed to have an effect on the crack driving force [23]. The goal of this work is hence to study the effect of low temperature material properties of steels, as expected in Arctic applications, on the crack driving force by performing finite element analyses. This effect is studied by simulating fracture tests of a single-edge-notched-tension (SENT) specimen with a material model where the temperature dependent material parameters can be changed. The CTOD is used as a measure of the crack driving force. A SENT specimen is studied because it is used as a fracture specimen to estimate fracture toughness of steels used for pipeline applications where other specimen types give unnecessarily conservative results, such as for girth welds in pipes [24, 25].

The results will be utilized to propose approximate CTOD models that can be used to estimate the crack driving force in a SENT specimen at low temperatures by using only tensile properties of the material. This can for instance also be useful for estimating the CTOD or maximum stress allowed in a cracked pipeline in Arctic climate.

2. Experimental work on low temperature tensile properties

The recent work by Ren et al. [9] and Østby et al. [23] has presented tensile properties of a 420 MPa steel at different temperatures ranging from 0 °C down to −90 °C. They tested both base material, weld metal and weld thermal simulated microstructure of steel. Smooth round specimens with gauge diameters between 10 mm and 12 mm were used for testing the base material, and

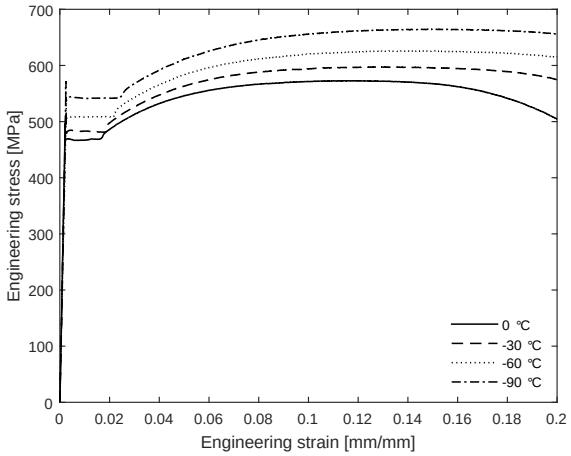

Figure 1: Engineering stress-strain curves of a 420 MPa steel at different temperatures. Taken from [9].

they were loaded with a strain rate of $8 \times 10^{-4}\,\mathrm{s}^{-1}$. An example of engineering stress-strain results is shown in Fig. 1.

The results in Fig. 1 show that both the yield strength and the Lüders strain increase with decreasing temperature. The yield strength and Lüders strain from 0 °C to −90 °C are ranging from approximate 470 MPa and 1.4 % to 540 MPa and 2.2 % respectively.

Tensile properties at low temperatures cannot always be obtained due to cost or practical reasons, and several corrections for calculating tensile properties at temperatures lower than room temperature are thus proposed in literature [9, 23, 26].

Ren et al. [9] introduced a modified version of the correction proposed by Østby et al. [26] based on their results from tensile tests on a 420 MPa steel:

$$\sigma_{y,T} = 420 + 0.73\left(\frac{10^5}{491 + 1.8T} - 137\right) \tag{1}$$

where $\sigma_{y,T}$ is the yield strength in MPa at temperature T in °C. They proposed in addition a relation between Lüders strain and temperature:

$$\varepsilon_L = 0.0142\exp(-0.005T) \tag{2}$$

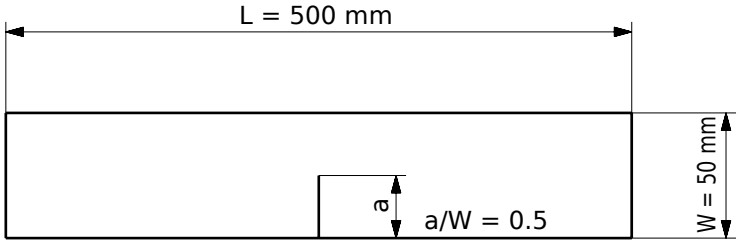

Figure 2: Illustration of a SENT specimen with dimensions.

where T is the temperature in °C and ε_L is the Lüders strain. Eqs. 1 and 2 are expected to be valid for the tested temperature range from $-90\,°C$ to $0\,°C$. The effect of the low temperature tensile properties on the crack driving force will be numerically studied in the following, where Eqs. 1 and 2 will be used to estimate the yield strength and Lüders strain present at different temperatures.

3. Material model and numerical procedure

The numerical simulations were performed using the commercial finite element program Abaqus 6.14 [27]. The finite element (FE) model studied is a two-dimensional plane strain SENT specimen. The symmetry is utilized by modelling only half of the specimen. The width of the specimen is 50 mm, and the other dimensions are determined using a recommended practice [25]: $L/W = 10$ and $a/W = 0.5$, where W is the specimen width, L is the specimen length, and a is the crack length as illustrated in Fig. 2.

Large plastic deformations are expected at the crack tip, and the crack is modelled as an initially blunted crack with a tip radius of 10 µm. The large-displacement formulation that accounts for nonlinear geometric effects (NLGEOM) is used in the analyses. The finite element mesh consists of 1355 8-node plane strain CPE8 elements. The mesh is refined around the crack tip where large strain gradients are expected, which is the primary area of interest in this study. There are 10 elements along the edge of the crack tip. The mesh and crack tip radius were determined based on a convergence study with varying mesh densities, element types and crack tip radii. The final finite element mesh

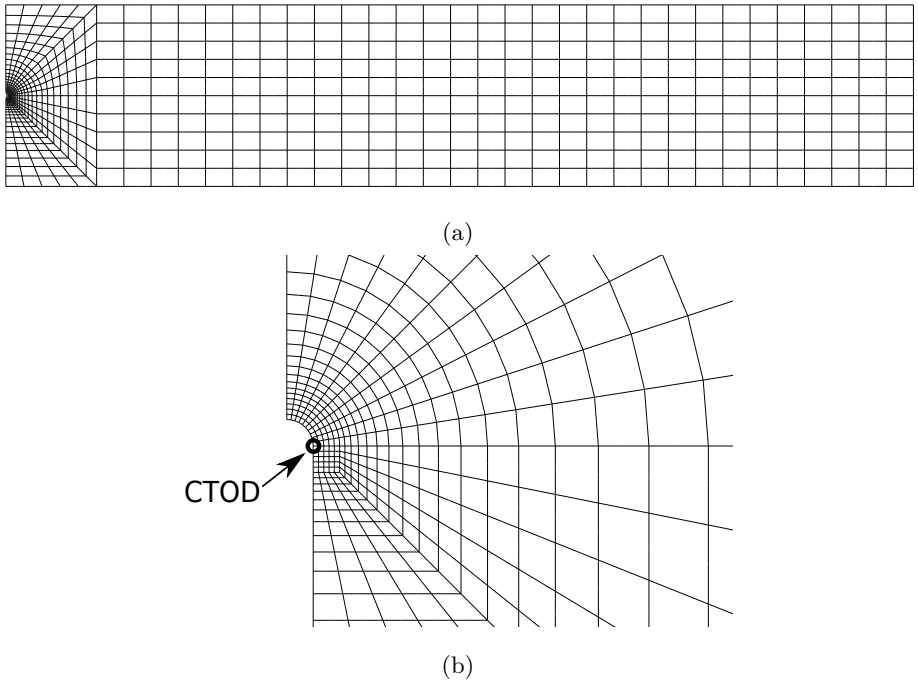

Figure 3: (a) Global and (b) local finite element mesh. The node where CTOD is measured is marked by the circle in (b).

is shown in Fig. 3.

A uniform displacement is applied on the end of the half specimen to simulate the tension of a clamped SENT specimen. The displacement is set as high as needed to make the ligament net section stress exceed the yield stress of the material.

An elastoplastic material model based on uniaxial tensile tests of the steel in [9] is used in the analyses. The material displays isotropic linear elasticity and J_2-plasticity with isotropic hardening, while an amount of Lüders straining is added in the transition between the elastic and plastic behavior. The Lüders behavior is modelled as a simplified horizontal Lüders plateau in the plastic stress-strain curve. There are many proposals for more realistic modelling of the Lüders instability in literature, which for instance include strain drops or strain softening [8, 17, 19, 20, 28–31]. In previous works done by O'Dowd [32],

Table 1: Constant material parameters.

E	ν	K	n
210 GPa	0.3	685 MPa	0.576

Nourpanah and Taheri [33], a Ramberg-Osgood fitting of material stress-strain curves was applied and showed that conservative estimation of fracture response can be obtained using this approach. In this paper, the simplified flat Lüders plateau is assumed, which is expected to give a better approximation to the material behavior in the present analysis.

This is verified by doing analyses using a material model similar to the model in [20]. The modelled stress-strain curve is fitted to true stress-strain data from the uniaxial tensile tests in [9], and it is then modified to create several similar materials with varying parameters such as yield stress and Lüders strain. The material can be described by

$$\sigma = \begin{cases} E\varepsilon & \text{if } 0 \leq \varepsilon < \frac{\sigma_y}{E} \\ \sigma_y & \text{if } \frac{\sigma_y}{E} \leq \varepsilon < \frac{\sigma_y}{E} + \varepsilon_L \\ \sigma_y + K\left(\varepsilon - \left(\frac{\sigma_y}{E} + \varepsilon_L\right)\right)^n & \text{if } \varepsilon \geq \frac{\sigma_y}{E} + \varepsilon_L \end{cases} \tag{3}$$

in uniaxial tension, where σ is the uniaxial stress, E is the Young's modulus, ε is the uniaxial strain, σ_y is the yield stress, ε_L is the Lüders strain, K is a strength coefficient and n is the strain hardening exponent. For loads and deformations in the two-dimensional plane, the Poisson's ratio ν is also needed. The yield stress and Lüders strain are the temperature dependent parameters to be studied. The constant material parameters are summarized in Table 1, where K and n are determined by fitting Eq. 3 to the true stress-strain data from the uniaxial tensile testing in [9]. Eq. 3 divides the stress-strain curve into three parts: the linear elastic part, Lüders plateau and plastic hardening, as illustrated in Fig. 4. As only quasi-static simulations are performed, there are no rate dependencies in the material model.

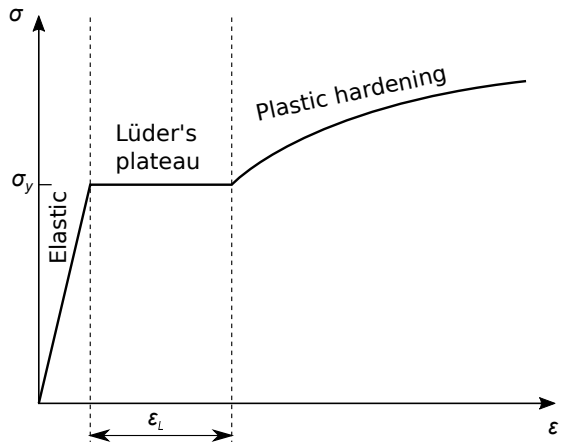

Figure 4: Illustration of a material model showing the three different parts of the stress-strain curve.

4. Results and discussion

To study how temperature dependent material properties affect the crack driving force, different analyses were performed where the parameters of interest were studied individually, and thereafter their combined effect was investigated. This study focuses on the effects of varying yield strength and Lüders strain on the CTOD. The CTOD is measured as twice the opening displacement of the fixed node in the transition point between the semicircular crack tip edge and the straight crack surface, as shown by the circle in Fig. 3b, which is equivalent to the initially 90 degree intercept method. The same procedure using a fixed node to calculate CTOD has been utilized in [34–38]. The results will be used to propose approximate CTOD models that can be utilized to estimate the CTOD based on given loadings and temperatures.

4.1. Effect of yield stress

The effect of yield stress was studied by keeping the other parameters constant. Analyses with different yield stresses were performed with different levels of Lüders strain. A total of 36 analyses were performed to produce the following results, where 6 different yield stress levels, 300, 400, 500, 600, 700 and 800 MPa,

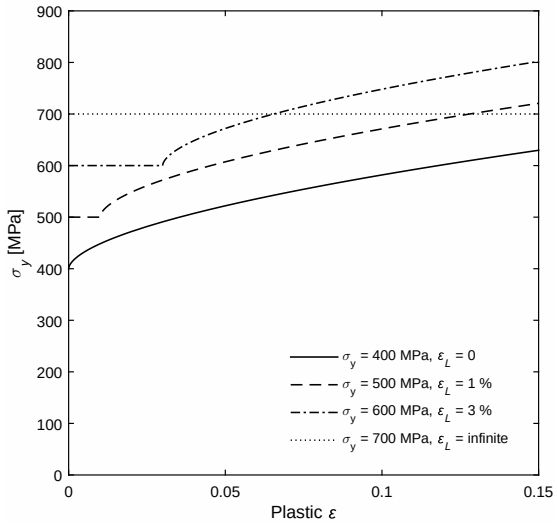

Figure 5: Examples of some of the model materials studied.

were tested with 6 different levels of Lüders strain ranging from 0 to infinite. Examples of plastic uniaxial material responses are shown in Fig. 5, where four materials with 400, 500, 600 and 700 MPa yield strength and 0, 1 %, 3 % and infinite Lüders strain respectively are displayed.

The CTOD results are plotted versus the gross stress level in each case in Fig. 6. The gross stress level is defined as σ_G/σ_y, where σ_G is the gross stress defined as $\sigma_G = F_{\|}/(Wt)$, where $F_{\|}$ is the longitudinal reaction forces at the specimen end, W is the specimen width and t is the specimen thickness. These results show that increasing yield stress results in increased CTOD at the same σ_G/σ_y. This can be expected as the same relative stress level corresponds to higher stresses and thus higher elastic strains in materials with higher yield strengths. This leads to a larger elastic deformation and hence a larger CTOD at the same relative stress level for a material with higher yield stress.

4.2. Effect of Lüders strain

The effect of the temperature dependent Lüders strain was studied by changing the amount of Lüders strain in the material model, while keeping the other parameters constant. This is the same as changing the length of the Lüders

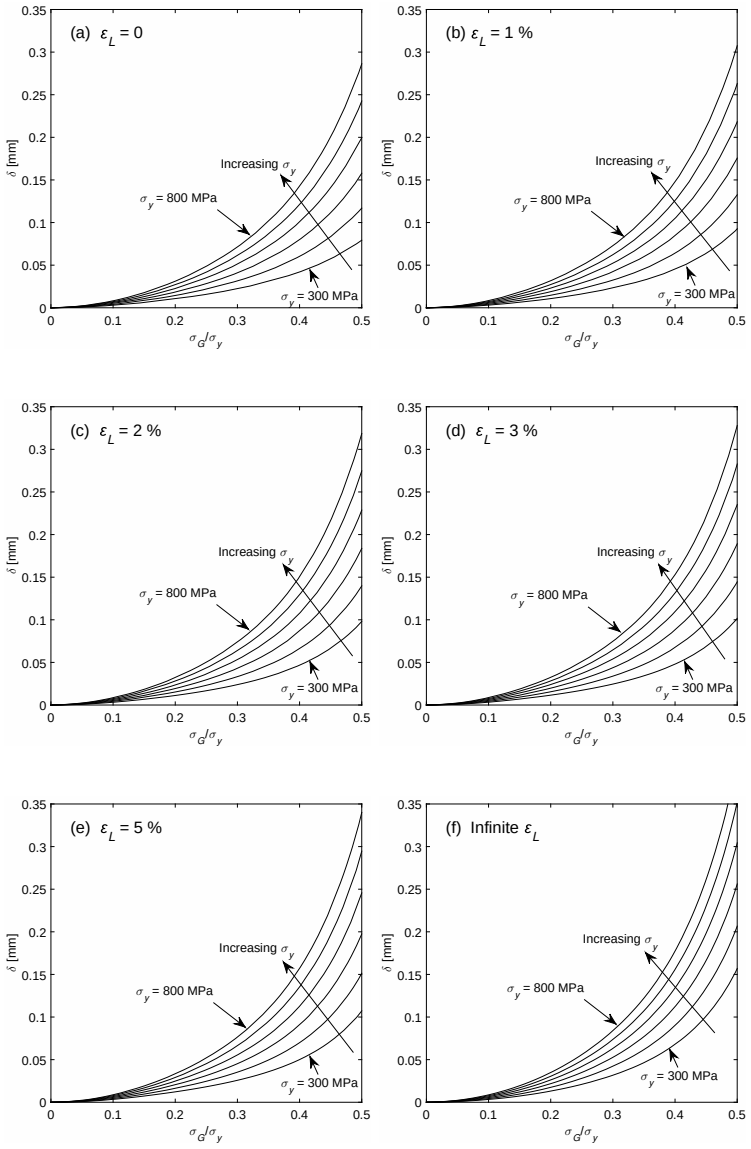

Figure 6: CTOD versus gross stress level with 300 MPa to 800 MPa yield strengths and Lüders strains ranging from 0 to infinite in (a) to (f) respectively.

plateau in the uniaxial stress-strain curve. A total of 36 analyses were performed to produce the following results, where 6 different Lüders strains, 0, 1, 2, 3, 5 % and infinite, were tested with 6 different levels of yield stress ranging from 300 to 800 MPa.

The results from the simulations are shown in Fig. 7, where the CTOD is plotted against the gross stress level. These are the same results as in Fig. 6, but rearranged so that the effect of Lüders strain can be more easily studied. The results indicate that increasing Lüders strain, for instance caused by decreasing temperature, yields a larger CTOD, and hence a larger crack driving force, for a given loading. This can be explained due to the larger plastic deformation allowed by a material with larger Lüders strain. Fig. 7 also indicates that the effect of Lüders strain on the CTOD is more evident at larger stress levels due to the difference in allowed plastic deformation. It should also be noted that the effect approaches a maximum for very large Lüders strains, as the curves approach the one for the material with inifinite Lüders strain. The material with infinite Lüders strain corresponds to a material which displays perfect plasticity.

4.3. Approximate CTOD model

The results from the previous sections clearly show that the tensile properties have an effect on the crack driving force. These results will be utilized to create an approximate model that can be used for estimating the crack driving force in terms of CTOD based on yield strength and Lüders strain. This model will later in this section be coupled to the effect of temperature on the yield strength and Lüders strain according to Eqs. 1 and 2. The model can thus be used to estimate the CTOD in a SENT specimen based on loading and temperature when the effect of temperature on the tensile properties are known.

Based on the results in the previous sections the following relation between CTOD and gross stress level is proposed:

$$\frac{\delta}{\delta_0} = b\left[\exp\left(d\frac{\sigma_G}{\sigma_y}\right) - 1\right] \tag{4}$$

where δ_0 is a reference CTOD equal to 0.25 mm, which is a minimum required

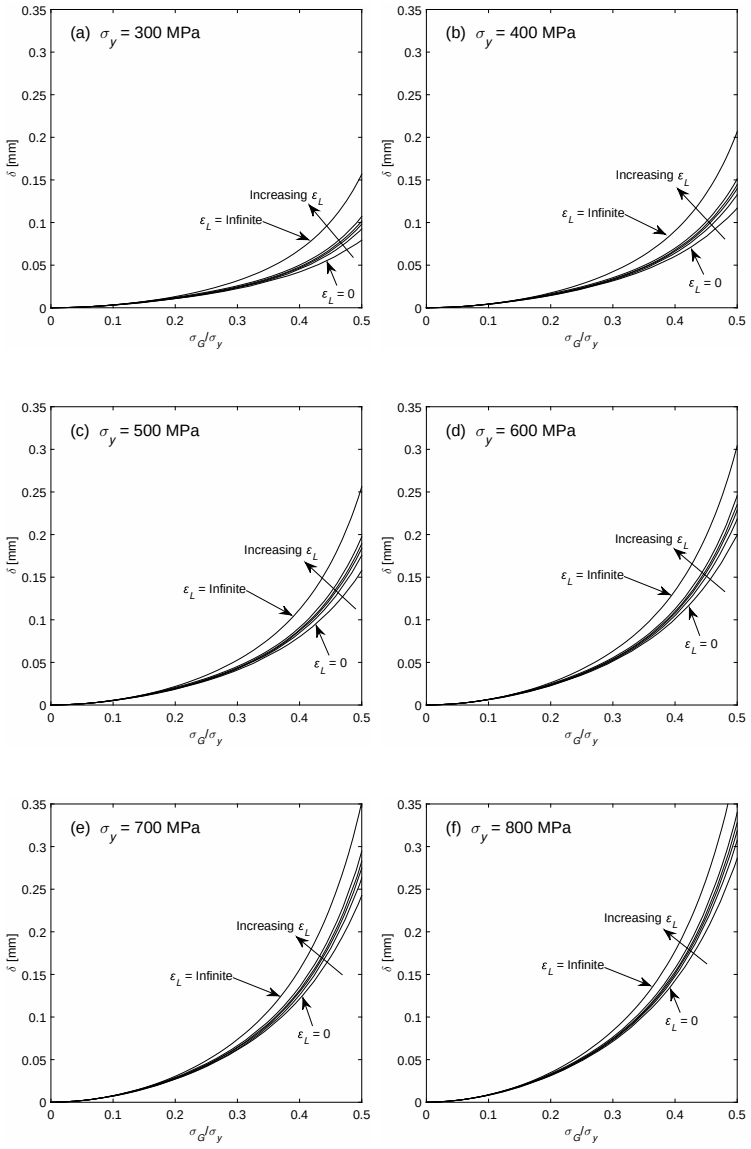

Figure 7: CTOD versus gross stress level with 0, 1 %, 2 %, 3 %, 5 % and infinite Lüders strains and yield strengths ranging from 300 MPa to 800 MPa in (a) to (f) respectively.

CTOD when applicable according to [39]. b and d are functions of yield stress and Lüders strain. Values for b and d in Eq. 4 were found by fitting the proposed relation to the numerical results shown in Figs. 6 and 7, and based on these results the following relation for b is proposed:

$$b = \begin{cases} \left(23.4\dfrac{\sigma_y}{\sigma_0} + 2.7\right) \times 10^{-3} & \text{if } \varepsilon_L = 0 \\ \left(23.2\dfrac{\sigma_y}{\sigma_0} - 1.1\right) \times 10^{-3} & \text{if } 0 < \varepsilon_L \leq 1\,\% \\ \left(21.6\dfrac{\sigma_y}{\sigma_0} - 0.6\right) \times 10^{-3} & \text{if } 1\,\% < \varepsilon_L \leq 5\,\% \end{cases} \tag{5}$$

where b is a function of the yield stress normalized by a reference stress (σ_0) equal to 420 MPa, which is the specified minimum yield strength (SMYS) for many construction steels. As Fig. 7 suggests, the effect of Lüders strain is evident, and it is thus accounted for in Eq. 5 by dividing the equation into three separate parts, where the first part is valid for materials showing no Lüders behavior, the second part is valid for Lüders strains below 1 %, and the third part is valid for larger Lüders strains up to 5 %. This partitioning of Eq. 5 helps estimating the CTOD more precisely for various levels of Lüders strain. The proposed relation for b as a function of σ_y/σ_0 is shown in Fig. 8 together with the values for b according to the fitting of Eq. 4 to the numerical results.

Based on the values for d found by fitting Eq. 4 to the numerical results, the following relation is proposed:

$$d = \begin{cases} -0.51\left(\dfrac{\sigma_y}{\sigma_0}\right)^2 + 1.97\dfrac{\sigma_y}{\sigma_0} + 4.52 & \text{if } 0 \leq \varepsilon_L < 1\,\% \\ -0.33\left(\dfrac{\sigma_y}{\sigma_0}\right)^2 + 1.17\dfrac{\sigma_y}{\sigma_0} + A & \text{if } 1\,\% \leq \varepsilon_L \leq 5\,\% \end{cases} \tag{6}$$

where d is a function of yield strength normalized by the reference stress of 420 MPa. d is dependent on the amount of Lüders strain, and A is a function of Lüders strain. Similar to Eq. 5, the partitioning of Eq. 6 into two Lüders strain ranges helps estimating the CTOD more precisely for various levels of Lüders strain. Based on the fitting of Eq. 6 to the values for d found by fitting Eq. 4

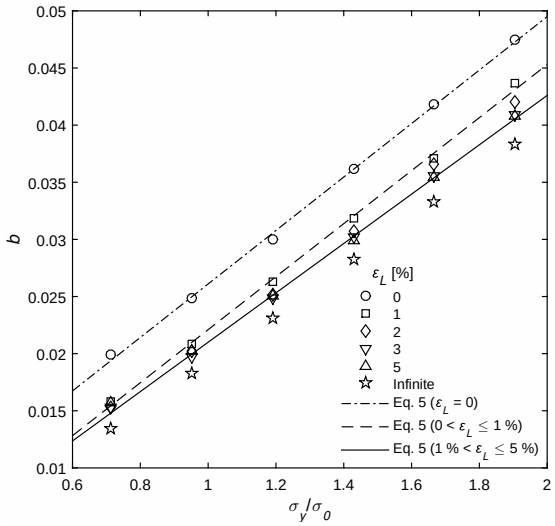

Figure 8: Proposed relations according to Eq. 5 as a function of yield strength normalized by a reference stress of 420 MPa together with the values for the b-parameter obtained by fitting the proposed relation in Eq. 4 to the numerical results shown in Figs. 6 and 7.

to the numerical results, the following relation between A and ε_L is proposed:

$$A = \frac{6.025}{1 + 0.106\exp(-58\varepsilon_L)} \tag{7}$$

The proposed relation between A and ε_L is shown in Fig. 9 together with the values for A, which were found by fitting the relation from Eq. 7 to the numerical results. The proposed relation for d in Eq. 6 using the calculated values for A according to Eq. 7 is shown in Fig. 10 as a function of yield stress normalized by the reference stress together with the values for d according to the fitting of Eq. 4 to the numerical results.

The model described by the proposed relations in Eqs. 4, 5, 6 and 7 are compared to numerical results by coupling the model to the effect of temperature on the tensile properties. This is done by varying the yield strength and Lüders strain in the model material according to Eqs. 1 and 2 respectively at four different temperatures. The temperatures used are the same as during the experimental tensile tests in [9]. The comparison between the estimated and the numerical results is shown in Fig. 11, where the normalized CTOD is plotted

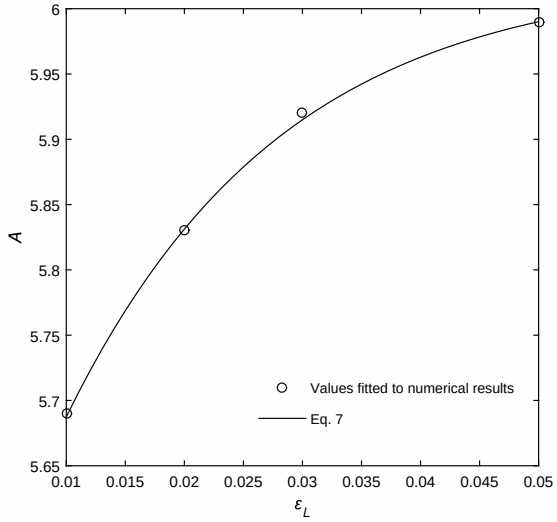

Figure 9: Comparison between Eq. 7 and the values for A from the fitting of Eq. 6 to the numerical results.

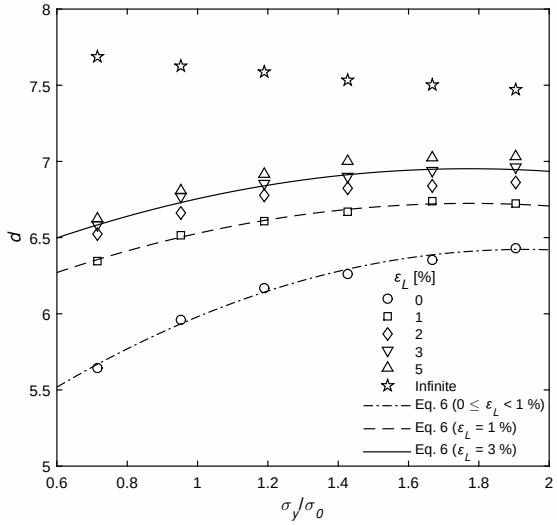

Figure 10: Proposed relations according to Eqs. 6 and 7 as a function of yield strength normalized by a reference stress of 420 MPa together with the values for the d-parameter obtained by fitting the proposed relation in Eq. 4 to the numerical results shown in Figs. 6 and 7.

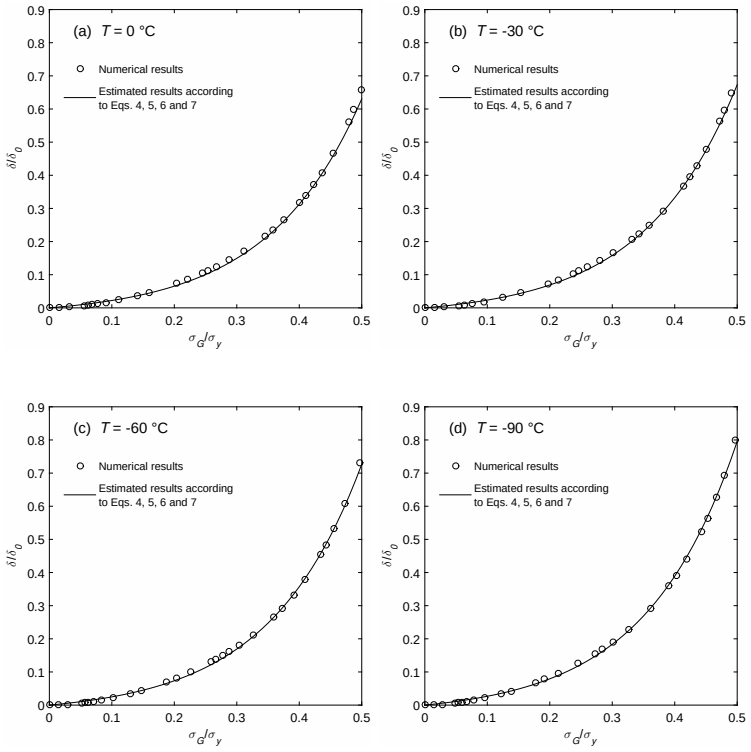

Figure 11: Proposed temperature dependent relation according to Eqs. 4, 5, 6 and 7 between CTOD and applied gross stress level in the SENT specimen compared to numerical results at (a) 0 °C, (b) −30 °C, (c) −60 °C and (d) −90 °C.

versus the applied gross stress level. The estimated results for the four different temperatures are compared in Fig. 12. The gross stress levels are calculated as the gross stress divided by the estimated yield stresses according to Eq. 1 at the respective temperatures.

Figs. 11 and 12 indicate that the proposed relations can be used to estimate the CTOD at different temperatures quite accurately for the material model used in this study. The proposed CTOD model utilizes known temperature dependent behavior of the yield strength and Lüders strain to estimate the CTOD in a SENT specimen at different temperatures and gross stress levels. The model may also be modified to estimate the CTOD for other geometries,

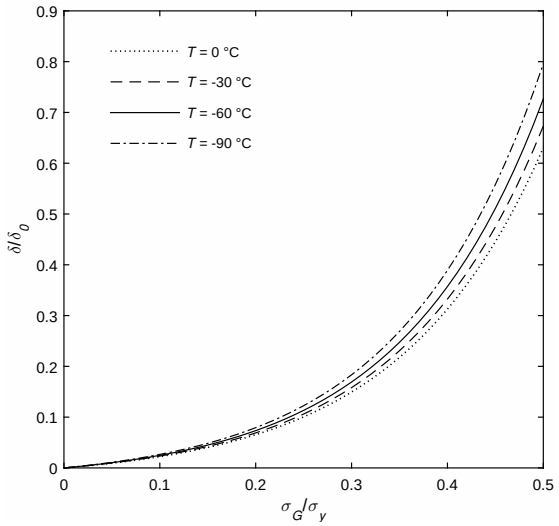

Figure 12: Comparison between CTOD curves estimated using the proposed CTOD model at four different temperatures.

such as for cracks in pipelines in Arctic conditions. The model should also be sufficient to use for other similar materials if their tensile behavior is comparable and the effect of temperature on the tensile behavior is known.

5. Conclusion

The effects of temperature dependent tensile properties on the crack driving force in a SENT specimen have been studied numerically, and an approximate model that predicts the CTOD based on tensile properties, temperature and loading is proposed. The SENT specimen studied has crack depth $a/W = 0.5$, and the material model is based on experimental results. The gross stress levels applied in this work are $\sigma_G/\sigma_y \leq 0.5$.

The yield strength and Lüders strain are both usually increasing with decreasing temperature. In this work it is shown that increasing yield strength results in increased crack driving force in terms of CTOD for given gross stress levels. It is also shown that increasing Lüders strain results in increased CTOD. The crack driving force is thus increasing with decreasing temperature at given

gross stress levels.

The proposed approximate CTOD model is based on the numerical results, and it is found to give quite accurate results when compared to numerical results using the same geometry, loading and material model as used in this work. The model may also be modified to predict the CTOD for other similar geometries and materials at different temperatures. This can for instance make it useful in estimating the CTOD based on temperature and loading for a crack in a pipeline in Arctic conditions.

The topics of this work can be further studied, where by other things the effect of geometry and crack tip constraint on the proposed model can be investigated, as only one geometry was studied in this work. This may result in a universal model that can be used to predict the crack driving force for many different geometries and applications. Also the effect of plastic hardening behavior can be studied in more detail, as this work only considers a single hardening curve for all material models.

Acknowledgements

The authors wish to thank the Research Council of Norway for funding through the Petromaks 2 Programme, Contract No.228513/E30. The financial support from ENI, Statoil, Lundin, Total, JFE Steel Corporation, Posco, Kobe Steel, SSAB, Bredero Shaw, Borealis, Trelleborg, Nexans, Aker Solutions, FMC Kongsberg Subsea, Kværner Verdal, Marine Aluminium, Hydro and Sapa are also acknowledged.

References

[1] D. L. Gautier, K. J. Bird, R. R. Charpentier, A. Grantz, D. W. Houseknecht, T. R. Klett, T. E. Moore, J. K. Pitman, C. J. Schenk, J. H. Schuenemeyer, Assessment of undiscovered oil and gas in the Arctic, Science 324 (5931) (2009) 1175–1179.

[2] O. M. Akselsen, E. Østby, B. Nyhus, Low temperature fracture toughness of X80 girth welds, in: The Twenty-second International Offshore and Polar Engineering Conference, International Society of Offshore and Polar Engineers, 2012, pp. 283–289.

[3] O. M. Akselsen, E. Østby, C. Thaulow, Low temperature toughness in SA welding of 420 MPa steel, in: The Twenty-first International Offshore and Polar Engineering Conference, International Society of Offshore and Polar Engineers, 2011, pp. 414–420.

[4] J.-H. Baek, Y.-P. Kim, W.-S. Kim, Y.-T. Kho, Effect of temperature on the charpy impact and CTOD values of type 304 stainless steel pipeline for LNG transmission, KSME International Journal 16 (8) (2002) 1064–1071.

[5] L. S. Costin, J. Duffy, The effect of loading rate and temperature on the initiation of fracture in a mild, rate-sensitive steel, Journal of Engineering Materials and Technology 101 (3) (1979) 258–264.

[6] A. S. Eldin, S. C. Collins, Fracture and yield stress of 1020 steel at low temperatures, Journal of Applied Physics 22 (10) (1951) 1296.

[7] E. Heier, E. Østby, O. M. Akselsen, Reeling installation of rigid steel pipelines at low temperature, in: The Twenty-third International Offshore and Polar Engineering Conference, International Society of Offshore and Polar Engineers, 2013, pp. 265–269.

[8] A. Marais, M. Mazière, S. Forest, A. Parrot, P. Le Delliou, Identification of a strain-aging model accounting for Lüders behavior in a C-Mn steel, Philosophical Magazine 92 (28-30) (2012) 3589–3617.

[9] X. Ren, H. O. Nordhagen, Z. Zhang, O. M. Akselsen, Tensile properties of 420 MPa steel at low temperature, in: The Twenty-fifth International Offshore and Polar Engineering Conference, International Society of Offshore and Polar Engineers, 2015, pp. 346–352.

[10] R. O. Ritchie, J. F. Knott, J. R. Rice, On the relationship between critical tensile stress and fracture toughness in mild steel, Journal of the Mechanics and Physics of Solids 21 (6) (1973) 395–410.

[11] C. F. Robertson, K. Obrtlik, B. Marini, Dislocation structures in 16MND5 pressure vessel steel strained in uniaxial tension at different temperatures from −196 °C up to 25 °C, Journal of Nuclear Materials 366 (1-2) (2007) 58–69.

[12] H. Sieurin, R. Sandström, Fracture toughness of a welded duplex stainless steel, Engineering Fracture Mechanics 73 (4) (2006) 377–390.

[13] W. A. Sorem, R. H. Dodds Jr, S. T. Rolfe, Effects of crack depth on elastic-plastic fracture toughness, International Journal of Fracture 47 (2) (1991) 105–126.

[14] M. L. Wilson, R. H. Hawley, J. Duffy, The effect of loading rate and temperature on fracture initiation in 1020 hot-rolled steel, Engineering Fracture Mechanics 13 (2) (1980) 371–385.

[15] A. H. Cottrell, B. A. Bilby, Dislocation theory of yielding and strain ageing of iron, Proceedings of the Physical Society of London Section A 62 (349) (1949) 49–62.

[16] G. T. Hahn, A model for yielding with special reference to the yield-point phenomena of iron and related bcc metals, Acta Metallurgica 10 (8) (1962) 727–738.

[17] J. F. Hallai, S. Kyriakides, Underlying material response for Lüders-like instabilities, International Journal of Plasticity 47 (2013) 1–12.

[18] D. H. Johnson, Lüders bands in RPV steel, PhD thesis, Cranfield University (2013).

[19] Y. Liu, S. Kyriakides, J. F. Hallai, Reeling of pipe with Lüders bands, International Journal of Solids and Structures 72 (2015) 11–25.

[20] M. Mazière, S. Forest, Strain gradient plasticity modeling and finite element simulation of Lüders band formation and propagation, Continuum Mechanics and Thermodynamics 27 (1-2) (2013) 83–104.

[21] N. Tsuchida, Y. Tomota, K. Nagai, K. Fukaura, A simple relationship between Lüders elongation and work-hardening rate at lower yield stress, Scripta Materialia 54 (1) (2006) 57–60.

[22] U. Zerbst, R. A. Ainsworth, H. T. Beier, H. Pisarski, Z. L. Zhang, K. Nikbin, T. Nitschke-Pagel, S. Munstermann, P. Kucharczyk, D. Klingbeil, Review on fracture and crack propagation in weldments - a fracture mechanics perspective, Engineering Fracture Mechanics 132 (2014) 200–276.

[23] E. Østby, O. M. Akselsen, M. Hauge, A. M. Horn, Fracture mechanics design criteria for low temperature applications of steel weldments, in: The Twenty-third International Offshore and Polar Engineering Conference, International Society of Offshore and Polar Engineers, 2013, pp. 315–321.

[24] B. Nyhus, M. L. Polanco, O. Ørjasæter, SENT specimens an alternative to SENB specimens for fracture mechanics testing of pipelines, in: ASME 2003 22nd International Conference on Offshore Mechanics and Arctic Engineering, American Society of Mechanical Engineers, 2003, pp. 259–266.

[25] Det Norske Veritas, Recommended practice DNV-RP-F108: Fracture control for pipeline installation methods introducing cyclic plastic strain (January 2006).

[26] British Standards Institution, BS 7910: Guide to methods for assessing the acceptability of flaws in metallic structures (2013).

[27] Dassault Systèmes Simulia Corp., Abaqus 6.14 (2014).

[28] T. Shioya, J. Shioiri, Elastic-plastic analysis of the yield process in mild steel, Journal of the Mechanics and Physics of Solids 24 (4) (1976) 187–204.

[29] H. Tsukahara, T. Iung, Finite element simulation of the Piobert–Lüders behavior in an uniaxial tensile test, Materials Science and Engineering: A 248 (1–2) (1998) 304–308.

[30] M. R. Wenman, P. R. Chard-Tuckey, Modelling and experimental characterisation of the Lüders strain in complex loaded ferritic steel compact tension specimens, International Journal of Plasticity 26 (7) (2010) 1013–1028.

[31] Y. T. Zhang, J. L. Qiao, T. Ao, Strain softening of materials and Lüders-type deformations, Modelling and Simulation in Materials Science and Engineering 15 (2) (2007) 147–156.

[32] N. P. O'dowd, Applications of two parameter approaches in elastic-plastic fracture mechanics, Engineering Fracture Mechanics 52 (3) (1995) 445 – 465.

[33] N. Nourpanah, F. Taheri, Development of a reference strain approach for assessment of fracture response of reeled pipelines, Engineering Fracture Mechanics 77 (12) (2010) 2337 – 2353.

[34] P. A. Eikrem, Z. L. Zhang, B. Nyhus, Effect of plastic prestrain on the crack tip constraint of pipeline steels, International Journal of Pressure Vessels and Piping 84 (12) (2007) 708–715.

[35] J. Liu, Z. L. Zhang, B. Nyhus, Residual stress induced crack tip constraint, Engineering Fracture Mechanics 75 (14) (2008) 4151–4166.

[36] C. Thaulow, E. Østby, B. Nyhus, Z. L. Zhang, B. Skallerud, Constraint correction of high strength steel: Selection of test specimens and application of direct calculations, Engineering Fracture Mechanics 71 (16-17) (2004) 2417–2433.

[37] J. Xu, Z. L. Zhang, E. Østby, B. Nyhus, D. B. Sun, Effects of crack depth and specimen size on ductile crack growth of SENT and SENB specimens

for fracture mechanics evaluation of pipeline steels, International Journal of Pressure Vessels and Piping 86 (12) (2009) 787–797.

[38] J. Xu, Z. L. Zhang, E. Østby, B. Nyhus, D. B. Sun, Constraint effect on the ductile crack growth resistance of circumferentially cracked pipes, Engineering Fracture Mechanics 77 (4) (2010) 671–684.

[39] Standard Norge, NORSOK M-120: Material data sheets for structural steels (2008).